

Magnetically driven loss of centrosymmetry in metallic $\text{Pb}_2\text{CoOsO}_6$

A. J. Princep,^{1,*} H. L. Feng,^{2,†} Y. F. Guo,^{3,‡} F. Lang,¹ H. M. Weng,^{4,5} P. Manuel,⁶ D. Khalyavin,⁶ A. Shenshyn,⁷ M. Rahn,¹ Y. H. Yuan,⁸ Y. Matsushita,⁸ S. J. Blundell,¹ K. Yamaura,^{8,§} and A. T. Boothroyd^{1,¶}

¹*Department of Physics, University of Oxford, Clarendon Laboratory, Parks Road, Oxford, OX1 3PU, United Kingdom*

²*Department of Chemistry, Rutgers University, New Brunswick, New Jersey, USA*

³*School of Physical Science and Technology, ShanghaiTech University, Shanghai 201210, China*

⁴*Beijing National Laboratory for Condensed Matter Physics,*

Institute of Physics, Chinese Academy of Sciences, Beijing 100190, China

⁵*Collaborative Innovation Center of Quantum Matter, Beijing, China*

⁶*ISIS Facility, Rutherford Appleton Laboratory, Chilton, Didcot, OX11 0QX, United Kingdom*

⁷*FRM-II, Technische Universität München, Garching 85747, Germany*

⁸*Superconducting Properties Unit, National Institute for Materials Science, 1-1 Namiki, Tsukuba, Ibaraki 305-0044, Japan*

(Dated: June 8, 2022)

We report magnetic, transport and neutron diffraction data showing that $\text{Pb}_2\text{CoOsO}_6$, a newly synthesized metallic double-perovskite with a centrosymmetric space group at room temperature, exhibits a continuous second-order phase transition at 45 K to a magnetically ordered state with a non-centrosymmetric space group. The absence of inversion symmetry is very uncommon in metals, particularly metallic oxides. In contrast to the recently reported ferroelectric-like structural transition in LiOsO_3 , the phase transition in $\text{Pb}_2\text{CoOsO}_6$ is driven by a long-range collinear antiferromagnetic order, with propagation vector $\mathbf{k} = (\frac{1}{2}, 0, \frac{1}{2})$, which relieves the frustration associated with the magnetic exchanges. This magnetically-driven loss of inversion symmetry represents a new frontier in the search for novel metallic behavior.

Metals whose crystal structure lacks a center of inversion symmetry have been attracting increasing interest owing to the novel phenomena they can exhibit, such as optical activity [1] and a highly anisotropic thermopower, (a desirable property of certain thermoelectric devices) [2]. Non-centrosymmetric metals having strong electronic correlations can support exotic emergent quasiparticles, including skyrmions in chiral magnets [3]. Non-centrosymmetric superconductors are of particular interest because they can have spin-polarized supercurrents and unconventional pairing states with mixed singlet-triplet character even in the absence of strong electronic correlations [4–6]. The key feature of non-centrosymmetric systems is a band splitting throughout much of momentum space caused by spin-orbit coupling (Dresselhaus splitting [7]) which leads to a non-trivial topology of the electronic wave functions and plays an essential role in all these phenomena.

Non-centrosymmetric metals (NCSM) are relatively uncommon. This is because conduction electrons can effectively screen the electric dipole formation which is generally associated with acentricity. In fact, there exist to date only around 30 known NCSM, of which only a handful are metallic oxides [2]. Nevertheless, oxides are particularly attractive for device applications due to their stability under typical operating conditions, so the discovery of more oxide NCSM would be of considerable interest.

Structural transitions in metallic oxides which remove the center of inversion symmetry have previously been observed in $\text{Cd}_2\text{Re}_2\text{O}_7$ [8] and LiOsO_3 [9]. The origin and nature of the transition in $\text{Cd}_2\text{Re}_2\text{O}_7$ is uncertain, but LiOsO_3 was found to be an example of what Ander-

son and Blount referred to as a ferroelectric metal, i.e. a metal having a continuous structural phase transition accompanied by the appearance of a polar axis and the disappearance of an inversion centre [10]. The phase transition in LiOsO_3 is driven by the ordering of Li ion displacements [9].

Here, we report we report structural, magnetic and transport measurements of $\text{Pb}_2\text{CoOsO}_6$, another metal that undergoes a phase transition to a non-centrosymmetric structure. In this case, however, we show that the structural phase transition is driven by magnetoelastic coupling to an antiferromagnetic order parameter which relieves the magnetic frustration of the higher symmetry phase, analogous to the behavior of a type-II multiferroic. This represents a new paradigm for obtaining NCSM using magnetic frustration as a key ingredient.

Polycrystalline and single crystal $\text{Pb}_2\text{CoOsO}_6$ was prepared by a high pressure method (see Supplementary Materials). The room temperature crystal structure of polycrystalline $\text{Pb}_2\text{CoOsO}_6$ was initially determined by synchrotron X-ray diffraction (XRD) (see Supplementary Materials). The structure found is the fully ordered double perovskite structure with space group of $\text{P}2_1/n$ (tilt pattern $a^-a^-c^+$ in the notation of Glazer [11]). The Co and Os atoms occupy the Wyckoff positions 2a and 2b, respectively, and the bond valence sums imply +2 and +6 valence states for the Co and Os atoms respectively [12, 13]. The refined crystal structure is depicted in Fig. 1(a). The degree of distortion from the cubic structure is indicated by the deviation of inter-octahedral Co-O-Os bond angles which are 180° in the ideal structure, but here we find them to be 168° , 172° , and 145° , re-

spectively, implying substantial buckling of the octahedral connections.

The temperature variation of the structure of $\text{Pb}_2\text{CoOsO}_6$ was investigated between 1.5 K and 300 K by neutron powder diffraction (NPD). Neutron diffraction experiments were performed on a 4g powder at the ISIS facility on the WISH diffractometer. Rietveld refinements were carried out using the FullProf suite [14] using the magnetic form factor for Os^{6+} determined by Kobayashi *et al.* [15]. Results of refinement against the NPD pattern at 300 K are fully consistent with the synchrotron XRD results. The lattice parameters decrease monotonically with temperature below 300 K until $T_N = 45$ K, below which the parameters a and b increase slightly while c decreases significantly for a small net reduction in the unit-cell volume [see Fig. 1(b)]. This abrupt change in behavior of the lattice parameters is typically indicative of a magnetoelastic structural distortion accompanying the magnetic order, as discussed below. We identify T_N with a bulk antiferromagnetic ordering transition, based on the neutron diffraction and muon spin rotation experiments presented below, as well as by the existence of characteristic signatures in other physical properties (see Fig. 2).

Fig. 2(a) presents the temperature dependence of the electrical resistivity ρ of $\text{Pb}_2\text{CoOsO}_6$ measured on a single crystal between 2 K and 300 K. The single crystal was confirmed to have the same crystal structure as the powder sample by single crystal XRD (see Supplementary Materials and Fig. S2). The resistivity displays an anomaly at T_N without altering its metallic character. Above T_N , ρ is roughly linear in T , whereas below T_N , ρ shows a Fermi liquid-like behavior. The drop in ρ below T_N is likely due to the reduction in scattering of the conduction electrons by paramagnetic moments as the system undergoes magnetic ordering. The dc magnetic susceptibility (χ vs. T) of $\text{Pb}_2\text{CoOsO}_6$, presented in Fig. 2(b), exhibits a sharp peak at T_N , implying that the transition has a magnetic origin. A Curie-Weiss fit to χ^{-1} in the paramagnetic region above 200 K (see Fig. S2a in Supplementary Materials) yields the Curie-Weiss temperature $\Theta_W \approx -106$ K, suggesting dominant antiferromagnetic (AFM) interactions and a $|\Theta_W/T_N| \approx 2.2$, indicative of weak magnetic frustration. The effective magnetic moment (μ_{eff}) per formula unit is approximately $4.9 \mu_B$.

Below T_N , additional peaks were observed in NPD patterns that could be indexed with a propagation vector $\mathbf{k} = (\frac{1}{2}, 0, \frac{1}{2})$ [see Fig. 1(b) upper and Fig. 3(a)]. There are four magnetic irreducible representations (irreps) that are compatible with $k = (\frac{1}{2}, 0, \frac{1}{2})$ in the space group $P2_1/n$ and these are the 1-dimensional irreps mY_1^+ , mY_2^+ , mY_1^- , and mY_2^- [16]. The “+” type irreps correspond to order on only the Co sites, and the “-” irreps to order on only the Os sites, and each irrep has a specific relation between the direction of the moments on the two equivalent metal sites. The allowed magnetic Bragg re-

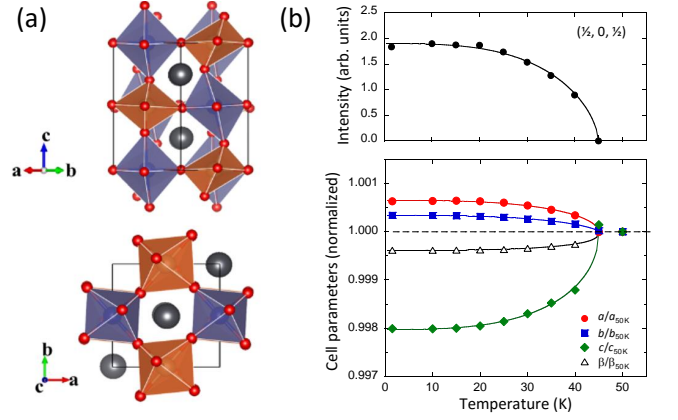


FIG. 1. (a) Crystallographic views of $\text{Pb}_2\text{CoOsO}_6$ along the [110] (left) and [001] (right) directions. The blue and brown octahedra represent CoO_6 and OsO_6 , respectively. The large grey solid spheres represent Pb. (b) (upper) temperature dependence of the fundamental magnetic reflection measured in neutron scattering and (lower) temperature dependence of the lattice parameters below the ordering temperature, relative to their value at T_N . Solid lines are a guide to the eye

flections vary with the choice of irrep, and inspection of the NPD data allowed us to constrain the possible irreps to mY_1^+ and mY_2^- . A model combining these two irreps was refined against NPD data from banks 2-9 of WISH. Fig. 3(a) shows data from banks 2 and 9 recorded at 1.5 K together with the refinement. The results of the refinement are tabulated in Table 1, and the magnetic structure is shown in Fig. 3(b).

The parameters describing the Co and Os moments are strongly correlated in the refinement and constraints are needed to reach convergence. Initial refinements performed with moments on only the Co sites or only the Os sites indicated that the magnetic structure is collinear and that the component along the b -axis (M_b) is very small. Thereafter, we set M_b to zero and performed fits as a function of the ratio of the moments on the Co and Os sites assuming all moments to be collinear. The substantial difference between the magnetic form factors of Co^{2+} and Os^{6+} provides a degree of sensitivity to the magnetic moment on each sublattice, and the best fit was found with approximately the same moment ($2.04 \mu_B$) on both Co and Os sites inclined at an angle of about 22 deg to the c axis. Fig. 3(a) shows data from banks 2 and 9 recorded at 1.5 K together with the refinement, and the insert shows the fit quality as the Os moment fraction is varied. The results of the refinement are tabulated in Table 1, and the magnetic structure is shown in Fig. 3(b).

The observation of a single magnetic transition indicates coincident order of the two sub-lattices, as observed recently in the osmate double-perovskite $\text{Sr}_2\text{FeOsO}_6$ [17]. Coincident order of coupled sublattices is to be expected unless the Co-O-Os superexchange was

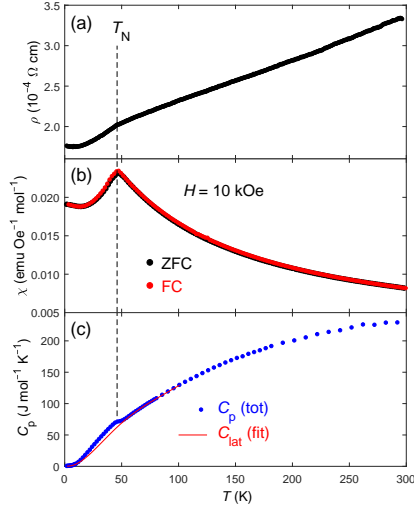


FIG. 2. Temperature dependence of bulk properties of $\text{Pb}_2\text{CoOsO}_6$. (a) Resistivity ρ of a single crystal. (b) Magnetic susceptibility χ of the polycrystalline sample. (c) Heat capacity C_p of the polycrystalline sample.

either highly frustrated or suppressed, in which case one expects two distinct magnetic transitions as appears to be the case in $\text{Sr}_2\text{CoOsO}_6$ [18].

The electronic structure of $\text{Pb}_2\text{CoOsO}_6$ was investigated by performing first-principles calculations, details of which are included in the supplementary Materials. The calculated density of states (DOS) indicates substantial contributions from both Co and Os d -electrons at the Fermi level, both of which are split into t_{2g} and e_g manifolds under the approximately octahedral crystal field (CF). The calculated local magnetic moments inferred from this are $2.46 \mu_B$ and $0.450 \mu_B$, on Co and Os respectively, consistent with the above approximate atomic configuration and with the range of possible experimental values indicated by NPD [see insert to Figure 2(a)].

As was noted earlier, below T_N the temperature dependence of the lattice parameters abruptly changes and they display an order-parameter-like behavior, suggesting that the lattice distortion is coupled to the magnetic

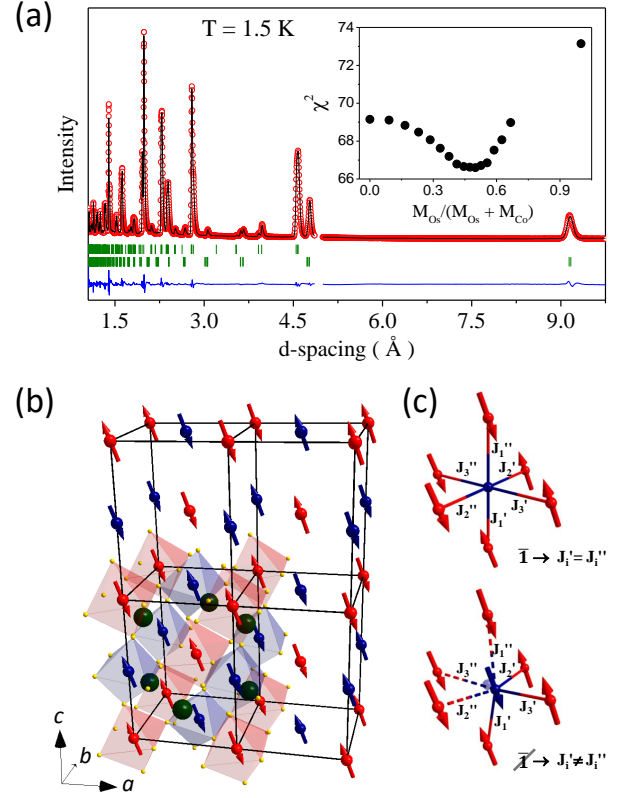


FIG. 3. Magnetic structure of $\text{Pb}_2\text{CoOsO}_6$. (a) Neutron diffraction data recorded in banks 2 and 9 of the WISH diffractometer are shown together with the Rietveld fit. The data are in red, the fit in black, and the difference in blue. The green tick marks indicate structural (upper) and magnetic (lower) Bragg peaks. The inset shows how the goodness-of-fit statistic χ^2 for the Rietveld fit varies as a function of the fraction of the total ordered moment that is located on the Os site. (b) Refined magnetic structure ($T < T_N$), with red and blue arrows as the Co^{2+} and Os^{6+} moments, respectively. The red and blue octahedra represent the oxygen coordination polyhedra, and the dark green spheres depict non-magnetic Pb^{2+} . (c) Removal of the center of inversion symmetry permits coupling between the magnetic order on the Co and Os sub-lattices.

order parameter. The magnetic structure refinement and DFT results provide evidence that there are ordered moments on both the Co and Os sites, and moreover, the refined magnetic structure does not possess a centre of symmetry. Any non-zero magneto-elastic coupling will then remove the centre of symmetry of the crystal structure, relieving frustration and reducing the space group symmetry of the structure to the (non-centrosymmetric) polar group P_n [19], with the corresponding Shubnikov group for the magnetic structure being P_a . Both Co and Os have a non-zero orbital angular momentum and so such coupling is expected to be non-negligible, and is indicated by the temperature-dependent variation of the lattice parameters described earlier [see Fig. 1(a)].

TABLE I. Refined values of the crystal and magnetic structures at 1.5K from neutron powder diffraction. Space group $P2_1/n$ (# 14, origin choice 2) $a = 5.63651(1)$ Å, $b = 5.58361(7)$ Å, $c = 7.82321(1)$ Å, and $\beta = 89.815(2)^\circ$. Magnetic moments on Co and Os sites were constrained to be equal. Final R values are: $R_{\text{nuc}} = 2.29\%$ and $R_{\text{mag}} = 7.91\%$. The lattice vectors of the Shubnikov group in the standard setting P_6c are related to the high temperature crystallographic space group $P2_1/n$ as $(-2, 0, 0)$, $(0, -1, 0)$, $(1, 0, 1)$ with an origin shift of $(0, \frac{1}{4}, 0)$.

Site	Wyck	x	y	z	B_{iso} (Å ²)
Pb	4e	0.0059(3)	0.5127(4)	0.2504(3)	0.45(4)
Co	2a	0	0	0	0.09(17)
Os	2b	0	0	0.5	0.18(6)
O1	4e	-0.0679(4)	-0.0088(7)	0.2592(4)	0.53(6)
O2	4e	0.2413(6)	0.2810(7)	0.0362(8)	0.55(12)
O3	4e	0.2834(6)	0.7651(6)	0.0365(8)	0.50(12)
Site		M_a	M_b	M_c	irrep
Co		-0.77(1)	0	1.89(1)	mY_1^+
Os		-0.77(1)	0	1.89(1)	mY_2^-

Although clear changes in structural elements of the diffraction pattern were observed on cooling through T_N , it proved impossible to refine a detailed model for the low temperature crystal structure owing to instabilities that resulted from the large number of free parameters.

The scenario of a magnetically-induced structural distortion described above requires magnetic order on both the Co and Os sublattices. As a further test of this picture we turned to zero-field muon-spin rotation (μ^+ SR), which is a local probe of magnetism. The μ^+ SR spectra reveal two dominant frequencies (see Supplementary Materials). To analyse the results we calculated the muon stopping sites by the DFT+mu approach [20, 21], and performed dipole field calculations based on the antiferromagnetic structure described earlier, varying the ratio of the ordered moments on the Co and Os sites assuming a fraction x of the total moment lies on the Os sites, and a fraction $1 - x$ lies on the Co sites. From this analysis (for more detail, see Supplementary Materials) we identify two scenarios which can plausibly explain our experimentally observed frequencies: either $0.5 < x < 0.6$ or $x \approx 1$. Both possibilities would lead to only two experimentally distinguishable frequencies, as is observed, with a ratio of the oscillation amplitudes of these two frequencies expected in the region of 1:1, in line with what is observed experimentally. Of these two possibilities, the scenario with $x \approx 1$ (i.e. the full moment is on the osmium site) is very unlikely. First, this scenario would require that the cobalt fails to order, contrary to other known double perovskites of mixed $3d$ - $5d$ cations, in which the $3d$ cation is either the only element that orders or the first to order by a significant margin. Second, the Os^{6+} in $\text{Pb}_2\text{CoOsO}_6$ would have to carry a moment (approx $4\mu_B$) substantially greater than that which has been observed

in any osmium containing compound to date; and indeed greater than should be possible even for an ideal $J = 2$ case (giving $3.6\mu_B$), which anyway does not seem to be favoured for Os due to covalency effects that are substantial compared to $3d$ and even $4d$ elements [22–24]. The likelihood of such a large moment on Os is further diminished by recent results on other $5d^2$ osmium double-perovskites $\text{Ba}_2\text{CaOsO}_6$ (ordered moment $< 0.2\mu_B$ [24]), $\text{Sr}_2\text{CoOsO}_6$ (ordered moment $1.8\mu_B$ [18]), Ca_3OsO_6 (moment estimated from Curie-Weiss fit $< 2\mu_B$ [25]), and both $\text{Sr}_2\text{MgOsO}_6$ and $\text{Ca}_2\text{MgOsO}_6$ (ordered moment $\approx 1.8\mu_B$ [26]). The weight of evidence overwhelmingly suggests that both the Os and Co ions carry an ordered moment in the magnetically ordered phase.

We conclude that the antiferromagnetic phase transition in $\text{Pb}_2\text{CoOsO}_6$, involving the simultaneous magnetic order on both the Co and Os sublattices, removes the centre of crystal symmetry and through magnetoelastic coupling relaxes the structure into the polar Shubnikov group P_6c . In $\text{Pb}_2\text{CoOsO}_6$, the spin-driven nature of the structural transition is reminiscent of a type-II multiferroic transition, in which magnetic order removes inversion symmetry. Unlike in multiferroics, however, the transition in $\text{Pb}_2\text{CoOsO}_6$ occurs entirely in the metallic state. Oxide NCSMs are still very rare, and the materials known up to now exist because the polar displacements are almost entirely decoupled from the conduction electrons. The magnetic mechanism for acentricity in $\text{Pb}_2\text{CoOsO}_6$ avoids this constraint and could provide a new route for the discovery of other oxide NCSMs and their associated novel phenomena. Thus, the phase transition we have illustrated in $\text{Pb}_2\text{CoOsO}_6$ could provide a new guiding principle for the future discovery of oxide NCSMs.

Acknowledgments

Two authors (AJP and HLF) contributed equally to this work. This research was supported in part by the World Premier International Research Center from MEXT; the Grants-in-Aid for Scientific Research (25289233) from JSPS; the Funding Program for World-Leading Innovative R&D on Science and Technology from JSPS; and United Kingdom Engineering and Physical Sciences Research Council (EPSRC). H.M.W. acknowledges the supports from NSF of China and the 973 program of China (No. 2011CBA00108 and 2013CB921700). YFG acknowledges the support of Shanghai Pujiang Program, grant No. 17PJ1406200. We performed the SXRD measurements with the approval of the NIMS beamline station (Proposal No. 2013B4503). This work was supported by EPSRC (UK) grants EP/N034872 and EP/N023803. The authors acknowledge the use of the University of

Oxford Advanced Research Computing (ARC) facility (<http://dx.doi.org/10.5281/zenodo.22558>).

* princep@physics.ox.ac.uk

† hf172@chem.rutgers.edu

‡ guoyf@shanghaitech.edu.cn

§ Yamaura.kazunari@nims.go.jp

¶ a.boothroyd@physics.ox.ac.uk

- [1] V. P. Mineev and Y. Yoshioka, Phys. Rev. B: Condens. Matter Mater. Phys. **81**, 094525 (2010).
- [2] D. Puggioni and J. M. Rondinelli, Nature Communications **5**, 3432 (2014).
- [3] S. Möhlbauer, B. Binz, F. Jonietz, C. Pfleiderer¹, A. R. A. Neubauer, R. Georgii, and P. Bni, Science **323**, 915 (2009).
- [4] S. Fujimoto, J. Phys. Soc. Jpn. **76**, 051008 (2007).
- [5] E. Bauer and M. Sigrist, *Non-Centrosymmetric Superconductors: Introduction and Overview* (Springer, Heidelberg, 2012).
- [6] K. V. Samokhin, Annals of Physics **359**, 385 (2015).
- [7] G. Dresselhaus, Physical Review **100**, 580 (1955).
- [8] I. A. Sergienko, V. Keppens, M. McGuire, R. Jin, J. He, S. H. Curnoe, B. C. Sales, P. Blaha, D. J. Singh, K. Schwarz, and D. Mandrus, Phys. Rev. Lett. **92**, 065501 (2004).
- [9] Y. Shi, Y. Guo, X. Wang, A. J. Princep, D. Khalyavin, P. Manuel, Y. Michiue, A. Sato, K. Tsuda, S. Yu, M. Arai, Y. Shirako, M. Akaogi, N. Wang, K. Yamaura, and A. T. Boothroyd, Nat. Mater. **12**, 1024 (2013).
- [10] P. W. Anderson and E. I. Blount, Phys. Rev. Lett. **14**, 217 (1965).
- [11] A. M. Glazer, Acta Cryst B **28**, 3384 (1972).
- [12] C. Ederer, T. Harris, and R. Kováčik, Phys. Rev. B **83**, 054110 (2011).
- [13] M. Azuma, K. Takata, T. Saito, S. Ishiwata, Y. Shimakawa, and M. Takano, J. Am. Chem. Soc. **127**, 8889 (2005).
- [14] J. Rodriguez-Carvajal, Physica B **192**, 55 (1993), <http://www.ill.eu/sites/fullprof/>.
- [15] K. Kobayashi, T. Nagao, and M. Ito, Acta Cryst. A **67**, 473 (1991).
- [16] S. C. Miller and W. F. Love, *Tables of Irreducible Representations of Space Groups and Co-Representations of Magnetic Space Groups* (Boulder: Pruett, 1967).
- [17] A. K. Paul, M. Reehuis, V. Ksenofontov, B. Yan, A. Hoser, D. M. Tbbens, P. M. Abdala, P. Adler, M. Jansen, and C. Felser, Phys. Rev. Lett. **111**, 167205 (2013).
- [18] R. Morrow, R. Mishra, O. D. Restrepo, M. R. Ball, W. Windl, S. Wurmehl, U. Stockert, B. Bchner, and P. M. Woodward, J. Am. Chem. Soc. **135**, 18824 (2013).
- [19] "Isotropy software suite," <http://iso.byu.edu>.
- [20] J. S. Möller, P. Bonfà, D. Ceresoli, F. Bernardini, S. J. Blundell, T. Lancaster, R. De Renzi, N. Marzari, I. Watanabe, S. Sulaiman, and M. I. Mohamed-Ibrahim, Physica Scripta **88**, 068510 (2013).
- [21] F. R. Foronda, F. Lang, J. S. Möller, T. Lancaster, A. T. Boothroyd, F. L. Pratt, S. R. Giblin, D. Prabhakaran, and S. J. Blundell, Physical Review Letters **114**, 017602 (2015).
- [22] S. Gangopadhyay and W. E. Pickett, Phys. Rev. B **91**, 045133 (2015).
- [23] A. E. Taylor, R. Morrow, D. J. Singh, S. Calder, M. D. Lumsden, P. M. Woodward, and A. D. Christianson, Phys. Rev. B **91**, 100406(R) (2015).
- [24] C. M. Thompson, J. P. Carlo, R. Flacau, T. Aharen, I. A. Leahy, J. R. Pollicemi, T. J. S. Munsie, T. Medina, G. M. Luke, and J. Munevar, J. Phys.: Condens. Matter **26**, 306003 (2014).
- [25] H. L. Feng, Y. Shi, Y. Guo, J. Li, A. Sato, Y. Sun, X. Wang, S. Yu, C. I. Sathisha, and K. Yamaura, Journal of Solid State Chemistry **201**.
- [26] Y. Yuan, H. L. Feng, M. P. Ghimire, Y. Matsushita, Y. Tsujimoto, J. He, M. Tanaka, Y. Katsuya, and K. Yamaura, Inorg. Chem. **54**, 3422 (2015).